Symmetry Lowering in Extreme-Electron-Density Perovskite Quantum Wells

Jack Y. Zhang, Jinwoo Hwang, Santosh Raghavan, and Susanne Stemmer

Phys. Rev. Lett. **110**, 256401 — Published 18 June 2013

DOI: 10.1103/PhysRevLett.110.256401

Symmetry lowering in extreme-electron-density perovskite quantum wells

Jack Y. Zhang, Jinwoo Hwang, Santosh Raghavan, and Susanne Stemmer

Materials Department, University of California, Santa Barbara, CA 93106-5050, USA

Abstract

We report on structural distortions in extreme-electron-density (~ 6×10^{14} cm^{-2}), confined quantum wells of $SrTiO_3$ embedded in $GdTiO_3$. Sr-column displacements are measured using high-angle annular dark-field imaging in scanning transmission electron microscopy. Using thick $SrTiO_3$ layers as a reference, orthorhombic-like Sr-site displacements are observed when $SrTiO_3$ quantum wells are thinner than 4 SrO layers, in precise agreement with an experimentally observed metal-to-insulator transition. It is shown that the structural displacements are absent in thicker quantum wells, even in the immediate proximity to the orthorhombic $GdTiO_3$. The results are discussed in the context of strong electron correlations in this system.

Unique physical phenomena occur in "Mott" insulators, in which electron-electron interactions are significant [1]. Prototypical Mott insulators often feature structural distortions, magnetic or charge ordering. For example, the rare earth titanates (ABO_3, where the A-site is a rare earth ion including Y, and B = Ti) exhibit oxygen octahedral tilts, or Ti-O-Ti bond angle distortions, away from the 180° angle in the ideal cubic perovskite structure. The insulating state is intimately coupled with the structural distortion, as the octahedral tilt lowers the bandwidth by reducing the charge transfer between neighboring Ti t_{2g} orbitals that occurs via the O 2p orbitals [2]. Furthermore, magnetic ordering temperatures, whether the ordering is antiferromagnetic or ferromagnetic, and the critical doping density needed for metallic conduction, are all correlated with the amount of tilt of the TiO_6 octahedron [2-4].

Thin film heterostructures allow for *separately* controlling the contributions of lattice distortions and electronic configuration to the insulating state. For example, octahedral tilts are modified by coherency strains imposed by the substrate, or by coupling across interfaces [5]. Electrostatic doping can be used to modulate carrier concentrations [6]. For example, $SrTiO_3$ can be electrostatically doped to high sheet carrier densities (~ ½ mobile electron per interface unit cell) by interfacing it with a rare earth titanate [7-9]. Signatures of electron correlations, including mass enhancement [10], were observed in narrow, metallic $SrTiO_3$ quantum wells bound by two such interfaces. This is remarkable because bulk $SrTiO_3$ is a band insulator with cubic symmetry. The thinnest quantum wells, which are 2 SrO layers wide on average, are *insulating* [10]. Recent density functional theory simulations indicate that oxygen octahedral tilts in the thinnest quantum wells are critical in promoting a Mott insulating

state [11]. Key to understanding the Mott physics of these extreme-electron-density quantum wells is, therefore, whether structural distortions indeed exist, and, if present, whether they are correlated with the insulating state, and what role the oxygen octahedral connectivity at the interface and electronic origins (high electron density) play in driving any distortion. To address these questions, we measure A-site cation displacements in $GdTiO_3/SrTiO_3/GdTiO_3$ structures, using high-angle annular dark-field (HAADF) scanning transmission electron microscopy (STEM). Although the studies are carried out on this specific system, we note that electrostatic doping of correlated materials is a subject of great current interest (see, e.g., refs. [12-16]). In this context, the $GdTiO_3/SrTiO_3$ system is an almost ideal model system, due to its relative chemical, electronic and structural simplicity, such as no pre-existing (bulk) structural distortions or electron correlations in the $SrTiO_3$.

$GdTiO_3$ is an orthorhombic distorted perovskite (space group *Pnma* [17]) with $a^+b^-b^-$ tilt in Glazer notation [18]. A feature of this tilt system is the two degrees of freedom of the A-site (along *x* and *z* in *Pnma*), allowing it to shift to a more favorable position to optimize its local oxygen coordination [19,20]. Therefore, while direct imaging of oxygen columns in HAADF is not yet possible, oxygen octahedra tilts in $a^+b^-b^-$ are directly related to A-site cation displacements, which can be measured. Bulk $SrTiO_3$ is cubic ($a^0a^0a^0$), having neither A-site displacements nor oxygen octahedral tilts.

Coherently strained $SrTiO_3$ and $GdTiO_3$ layers were grown on (001) $(La_{0.3}Sr_{0.7})(Al_{0.65}Ta_{0.35})O_3$ (LSAT), as described elsewhere [21]. Figure 1(a) shows a schematic of the sample. $GdTiO_3$ layers were 4 nm thick, while the $SrTiO_3$ thickness was varied from 1 SrO layer to 8 SrO layers. The structure had a 10 nm $SrTiO_3$ buffer and

cap, respectively. The $SrTiO_3$ quantum well thicknesses matched those in the electrical studies [10], except here they were in a single sample. This allowed for recording all data in a single session, thus reducing effects from any variability in microscope conditions. Cross-section samples were prepared by focused ion beam (5 kV Ga ions) and imaged on an FEI Titan S/TEM with a field-emission source and super-twin lens (C_s = 1.2 mm) operated at 300 kV. The convergence semi-angle was 9.6 mrad. All images analyzed had a 1024×1024 frame size recorded at the same magnification, with a dwell time of 30 μs to reduce effects from drift, while retaining a high signal-to-noise ratio. Centroid positions of each atom column were determined using a custom MATLAB algorithm [22]. Position averaged convergent beam electron diffraction (PACBED) [23] was used for precise tilt alignment. PACBED patterns were simulated using Kirkland's frozen phonon multislice code [24]. Figures 1(b-d) show representative HAADF images, discussed in more detail below. The nature of the AO layer (SrO vs. GdO) can be unambiguously identified from the image intensities.

The preferred orientation for $GdTiO_3$ on LSAT is $(110)_o \| (001)_c$, where the subscripts indicate the orthorhombic or cubic unit cells, respectively [21]. Orientation variants that are related by a 90° rotation about $[001]_c$ are expected [25,26], see Fig. 2(a). These will be projected along $[110]_o$ and $[001]_o$, respectively, in cross section samples imaged parallel to $\langle 100 \rangle_{\mathrm{LSAT}}$. Figure 2(b) shows the $GdTiO_3$ unit cell viewed along $[110]_o$ and $[001]_o$, and simulated and experimental PACBED patterns for these orientations. The sensitivity of PACBED to structural distortions has been demonstrated previously [26-28]. The PACBED patterns of the two orientation variants are distinct.

Reasonable agreement between experimental and simulated PACBED indicates that the $GdTiO_3$ has close to bulk-like symmetry. We note that under compressive in-plane strain, the tilt system should be more accurately $a^+a^-c^-$ [29]. The difference lies in the precise values for the tilt angles, which are not the subject of this study.

Quantitative analysis of the A-site displacements was performed on domains viewed along $\left[110\right]_o$, as they cannot be resolved along $\left[001\right]_o$ [see Fig. 2(b)]. A deviation angle, (180° - θ), serves as a measure of the displacement, where θ is the angle formed between three successive A-site cations (centroid positions), see Fig. 1(c). Figure 3 shows the deviation angle for each AO layer, obtained by averaging angles from 18 separate images. Shaded (blue) regions indicate the $GdTiO_3$ layers, easy to identify by their higher intensity in the HAADF images. The 10 nm $SrTiO_3$ cap and buffer (left and rightmost $SrTiO_3$ regions in Fig. 3), serve as a reference and estimate of the systematic error. The deviation angle in these layers is not quite zero, as expected for a cubic perovskite, but close to 1.5°, due to a combination of scan distortions, sample drift, and system noise, which alter the atomic centroid positions from a perfect line. While the 8 SrO and 4 SrO quantum wells are bulk-like, the Sr columns in the 1 and 2 SrO layer quantum wells exhibit large displacements, (180° - θ) ~ 6°. The differences can easily be seen in the HAADF images in Fig. 1, which show representative sections showing Sr column displacements in the 2 SrO quantum well [red line in Fig. 1(b)], and the absence of Sr column displacements in the first SrO layer at the interface between $GdTiO_3$ and the $SrTiO_3$ buffer [Fig. 1(c)]. The Sr column displacements can also be detected using Fourier transforms (FTs) of the images. Figure 4 shows HAADF images of the 8, 4, and 2 SrO layer quantum wells, along with FTs of a 64×1024 pixel region in the center of

each quantum well (corresponding to a width of 2 SrO layers). Integrated intensity profiles of each FT are shown in Fig. 4(c). Extra half-order peaks appear in the FT of the 2 SrO quantum well (see arrows), which are not observed in quantum wells thicker than 2 SrO layers. The extra peaks are due to Sr displacements parallel to the growth direction.

Because of the need to maintain oxygen connectivity across an interface [5], structural adjustments are expected in either the $GdTiO_3$ or $SrTiO_3$, or both, at the interface. As can be seen from Fig. 3, these occur mostly in the $GdTiO_3$, provided that the adjacent $SrTiO_3$ is thicker than 4 SrO layers. While the deviation angle in the interior of the $GdTiO_3$ layers is close to bulk (16.3° in the $\left[110\right]_o$ projection), ~ 2 - 3 GdO layers adjacent to $SrTiO_3$ show reduced Gd column displacements. This suggests that the TiO_6 octahedra in $GdTiO_3$ in the interface region are closer to 180°. The fact that interfacial connectivity constraints are largely accommodated in the $GdTiO_3$ indicates "softer" bond angles than in $SrTiO_3$. The reduced tilts of interfacial TiO_6 octahedra in the $GdTiO_3$ will almost certainly influence the local magnetic properties, which will be the subject of a future study.

We next discuss the $SrTiO_3$ quantum wells with 1 and 2 SrO layers, respectively. Unlike for thicker wells, Sr sites are significantly displaced in these layers, indicating a transition to an orthorhombic-like $a^+b^-b^-$ tilt system. In contrast to the changes in the displacements of the interfacial GdO layers, it appears that this is not (entirely) a consequence of interfacial connectivity, because (*i*) the GdO layers adjacent to them still show reduced Gd displacements, indicating that the need to maintain interfacial octahedral connectivity is still accommodated largely by the $GdTiO_3$, and (ii) SrO layers in thicker $SrTiO_3$ have bulk displacements, even when immediately adjacent to $GdTiO_3$.

It should also be stressed that the deviation angle in the 2 SrO layer should not be attributed to interdiffusion. While interfacial roughness is present, its effect on the deviation angle should apply equally at all $SrTiO_3/GdTiO_3$ interfaces. This is clearly not the case, as the SrO layers immediately adjacent to a $GdTiO_3$ in thicker $SrTiO_3$ films show bulk angles [Figure 3, points labeled X; also Fig. 1(c)]. An exception is layers where $SrTiO_3$ is grown on top of $GdTiO_3$ (points labeled Y). A small increase in deviation angle in the first SrO layer can be detected in this case, due to roughness at this interface (relative to one where $GdTiO_3$ is grown on $SrTiO_3$). Differences in roughness of α/β versus β/α interfaces are extremely common in epitaxy. For this reason, the nominal 4 SrO layer in Fig. 3 contains five data points, due to an extra mixed layer in some images. The deviation angle in this intermixed layer is much smaller than it is in the 2 SrO quantum wells. Extra GdO layers are also present in the first $GdTiO_3$ layer on top of the $SrTiO_3$ film buffer, again, due to limitations in controlling one atomic layer in the presence of steps and roughness, even though the sample thickness was small (20 -30 nm estimated from PACBED). It should be noted that these limitations do not impact any of the prior analysis, and only serve to support the conclusion that the 2 SrO deviation angle is a significant measurement and not a result of interfacial disorder.

Given that interface roughness is not the origin of the Sr displacements in the thinnest quantum wells, this points to a connection between electron correlations at extreme densities in the thinnest wells, and the observed symmetry-lowering. Although the electrons are localized in the 1 SrO and 2SrO quantum wells, Hall measurements indicate that these quantum wells still contain the entire electron density of ~ 6×10^{14} cm^{-2}, or one electron shared between three TiO_2 planes in the 2 SrO layer

quantum well [10,30,31]. Quantum wells with thicker $SrTiO_3$, having a lower 3D electron density, are metallic [10]. The results show that the metallic state has no Sr displacements and octahedral tilts; conversely, the insulating state is correlated with large Sr displacements and octahedral tilts. *The observed symmetry-lowering, most likely an orthorhombic-like distortion, occurs at the thickness for which the metal-to-insulator transition is observed in DC transport.* The results show that similar to bulk RTiO$_3$ Mott insulators, the transition to the insulating state is accompanied by a reduction of symmetry. The results support true "Mott" physics, controlled by on-site repulsive interaction at large electron densities, in these quantum wells.

Bulk $SrTiO_3$, even in its tetragonal low-temperature phase, does not exhibit Sr displacements. Compressively strained $SrTiO_3$ undergoes a phase transition to a structure that is similar to that for the bulk tetragonal phase [32]; thus no A-site displacements are expected due to the compressive film strain. We compared deviation angles in strained and compressively strained $SrTiO_3$ films and could find no difference. In bulk RTiO$_3$, A-site displacements are correlated with tilts of the TiO_6 octahedra. The deviation angle in the 2 SrO well (~ 6°) is significantly smaller than that of any RTiO$_3$ (ranging from 10.5° to 16.9° in $LaTiO_3$ and $YTiO_3$, respectively) [17]. Using empirical relationships between A-site cation displacements along $\left[110\right]_o$ and Ti-O-Ti bond angles in the RTiO$_3$ series [17], and interpolation to the cubic structure (0° deviation angle, 180° Ti-O-Ti angle), yields a Ti-O-Ti bond angle of ~160 ± 5° for the 2 SrO layer quantum well. In bulk RTiO$_3$, the activation energy for polaronic transport decreases with increasing Ti-O-Ti angle, with the lowest activation energy (~ 0.025 eV) measured for $LaTiO_3$ (Ti-O-Ti angle of 154°) [4]. The activation energy measured for the 2 SrO well is 0.02 eV [10],

consistent with the larger angle. Caution should, however, be applied in further comparisons with bulk $R\mathrm{TiO_3}$ due to differences in bonding, interfacial coupling, two-dimensionality etc. Furthermore, disorder almost certainly plays a role in the transition to the insulating state [10]. Future studies should establish the magnetic and/or charge ordering states (if present) in these quantum wells.

Finally we note that quantification of the oxygen octahedral tilts in the $\mathrm{SrTiO_3}$ quantum wells interface should be possible with PACBED. Such studies are currently underway [33]. However, we found PACBED in these structures more challenging than for the nickelate superlattices studied previously [27,28]. The dimensions of 2 SrO quantum wells along the growth direction are smaller than a single orthorhombic unit cell, and PACBED requires at least one unit cell. The surface of TEM samples containing $\mathrm{GdTiO_3}$ tends to be less ideal, which causes a background in the PACBED pattern and hinders quantification. Further development of the technique to overcome these issues is necessary.

Acknowledgements

The authors thank Leon Balents, Ru Chen, Jim Allen, Lars Bjalle, Anderson Janotti and Chris van de Walle for discussions. J.Y.Z. and J. H. were supported through DOE (award no. DE-FG02-02ER45994). S.S. and S.R. thank DARPA for support (award no. W911NF-12-1-0574). J.Y.Z. was supported also by the Department of Defense through an NDSEG fellowship. This work made use of facilities from the Center for Scientific Computing at the California Nanosystems Institute (NSF CNS-0960316) and the UCSB Materials Research Laboratory, an NSF-funded MRSEC (DMR-1121053).

References

[1] N. F. Mott, Proc. Phys. Soc. London Sec. A **62**, 416 (1949).

[2] M. Imada, A. Fujimori, and Y. Tokura, Rev. Mod. Phys. **70**, 1039 (1998).

[3] M. Mochizuki and M. Imada, New J. Phys. **6**, 154 (2004).

[4] H. D. Zhou and J. B. Goodenough, J. Phys.: Condens. Matter **17**, 7395 (2005).

[5] J. M. Rondinelli, S. J. May, and J. W. Freeland, MRS Bull. **37**, 261 (2012).

[6] C. H. Ahn, A. Bhattacharya, M. Di Ventra, J. N. Eckstein, C. D. Frisbie, M. E. Gershenson, A. M. Goldman, I. H. Inoue, J. Mannhart, A. J. Millis, et al., Rev. Mod. Phys. **78**, 1185 (2006).

[7] P. Moetakef, T. A. Cain, D. G. Ouellette, J. Y. Zhang, D. O. Klenov, A. Janotti, C. G. Van de Walle, S. Rajan, S. J. Allen, and S. Stemmer, Appl. Phys. Lett. **99**, 232116 (2011).

[8] S. S. A. Seo, W. S. Choi, H. N. Lee, L. Yu, K. W. Kim, C. Bernhard, and T. W. Noh, Phys. Rev. Lett. **99**, 266801 (2007).

[9] S. Okamoto and A. J. Millis, Nature **428**, 630 (2004).

[10] P. Moetakef, C. A. Jackson, J. Hwang, L. Balents, S. J. Allen, and S. Stemmer, Phys. Rev. B. **86**, 201102(R) (2012).

[11] R. Chen, S. Lee, and L. Balents, Phys. Rev B **87**, 161119(R) (2013).

[12] T. S. Santos, B. J. Kirby, S. Kumar, S. J. May, J. A. Borchers, B. B. Maranville, J. Zarestky, S. Velthuis, J. van den Brink, and A. Bhattacharya, Phys. Rev. Lett. **107**, 167202 (2011).

[13] M. Nakamura, A. Sawa, H. Sato, H. Akoh, M. Kawasaki, and Y. Tokura, Phys. Rev. B **75**, 155103 (2007).

[14] T. Higuchi, Y. Hotta, T. Susaki, A. Fujimori, and H. Y. Hwang, Phys. Rev. B **79**, 075415 (2009).

[15] F. Y. Bruno, R. Schmidt, M. Varela, J. Garcia-Barriocanal, A. Rivera-Calzada, F. A. Cuellar, C. Leon, P. Thakur, J. C. Cezar, N. B. Brookes, et al., Adv. Mater. **25**, 1468 (2013).

[16] J. Chakhalian, J. W. Freeland, H. U. Habermeier, G. Cristiani, G. Khaliullin, M. van Veenendaal, and B. Keimer, Science **318**, 1114 (2007).

[17] A. C. Komarek, H. Roth, M. Cwik, W. D. Stein, J. Baier, M. Kriener, F. Bouree, T. Lorenz, and M. Braden, Phys. Rev. B **75**, 224402 (2007).

[18] A. M. Glazer, Acta Cryst. B **28**, 3384 (1972).

[19] P. M. Woodward, Acta Crystallogr. B **53**, 32 (1997).

[20] P. M. Woodward, Acta Crystallogr. Sect. B **53**, 44 (1997).

[21] P. Moetakef, D. G. Ouellette, J. Y. Zhang, T. A. Cain, S. J. Allen, and S. Stemmer, J. Cryst. Growth **355**, 166 (2012).

[22] J. M. LeBeau and S. Stemmer, Ultramicroscopy **108**, 1653 (2008).

[23] J. M. LeBeau, S. D. Findlay, L. J. Allen, and S. Stemmer, Ultramicroscopy **110**, 118 (2010).

[24] E. J. Kirkland, Advanced Computing in Electron Microscopy, 2nd ed. (Springer, New York, 2010).

[25] D. O. Klenov, W. Donner, B. Foran, and S. Stemmer, Appl. Phys. Lett. **82**, 3427 (2003).

[26] P. Moetakef, J. Y. Zhang, S. Raghavan, A. P. Kajdos, and S. Stemmer, J. Vac. Sci. Technol. A **31**, 041503 (2013).

[27] J. Hwang, J. Y. Zhang, J. Son, and S. Stemmer, Appl. Phys. Lett. **100**, 191909 (2012).

[28] J. Hwang, J. Son, J. Y. Zhang, A. Janotti, C. G. Van de Walle, and S. Stemmer, Phys. Rev. B **87**, 060101 (2013).

[29] A. Vailionis, H. Boschker, W. Siemons, E. P. Houwman, D. H. A. Blank, G. Rijnders, and G. Koster, Phys. Rev. B **83**, 064101 (2011).

[30] D. G. Ouellette, T. A. Cain, J. Zhang, C. Jackson, S. Stemmer, and S. J. Allen, Unpublished (2013).

[31] Note that the exact distribution of the electrons over the TiO_2 layers will depend on factors such as band offsets and structural distortions, and the electrons may not distribute uniformly over the three layers.

[32] F. Z. He, B. O. Wells, and S. M. Shapiro, Phys. Rev. Lett. **94**, 176101 (2005).

[33] It should be noted that direct imaging of oxygen columns by aberration-corrected bright-field STEM or phase contrast imaging may not provide significantly more information: in $GdTiO_3$, along $[110]_o$, out-of-phase tilts cause the oxygen atom columns to split by 0.83 Å [see Fig. 2(b)]. As these tilts are much smaller in the $SrTiO_3$ quantum wells, they are likely beyond the resolution of even an aberration corrected instrument. Along $[001]_o$ in-phase tilts of O columns could potentially be resolved, although the close proximity to the Gd columns may make this difficult.

Figure Captions

Figure 1 (color online): (a) Schematic of the sample. $SrTiO_3$ layer thicknesses are indicated on the right (in units of SrO layers). (b) HAADF image of 2 SrO layers embedded in $GdTiO_3$ showing Sr column displacements. The red line is a guide to the eye. (c) HAADF image of the first $SrTiO_3$-buffer/$GdTiO_3$ interface showing Gd displacements parallel to the growth direction. The $GdTiO_3$ appears bright due to the larger atomic number of Gd. The angle θ (solid lines) is measured between three successive A-site cations. The first SrO row shows no Sr displacements (dashed line). (d) Lower magnification HAADF STEM image of the sample.

Figure 2 (color online): (a) $(110)_o \| (001)_c$ orientation of orthorhombic $GdTiO_3$ cell (solid black outline) on cubic LSAT (blue shaded). Projections are shown along $\lfloor 110 \rfloor_o$ (left) and $\lfloor 001 \rceil_o$ (right). Both occur within one cross-section sample due to domain formation. (b) Projected views of $GdTiO_3$ along $\lfloor 110 \rceil_o$ (top) and $\lfloor 001 \rceil_o$ (bottom), respectively, along with simulated and experimental PACBED patterns from these projections. The contrast in experimental patterns was adjusted to match background intensities of simulated patterns.

Figure 3 (color online): (a) Measured deviation angle, 180° – θ, of each AO layer in the sample. The error bars represent the standard error of the mean.

Figure 4 (color online): (a) HAADF STEM images of 8 SrO, 4 SrO and 2 SrO quantum wells. (b) FT of the center 2 SrO layers (64×1024 pixel region) from each quantum well and (c) integrated intensity profiles of the FT. Extra peaks appear in the FT from the 2 SrO quantum well, indicated by arrows, which are absent in thicker layers.

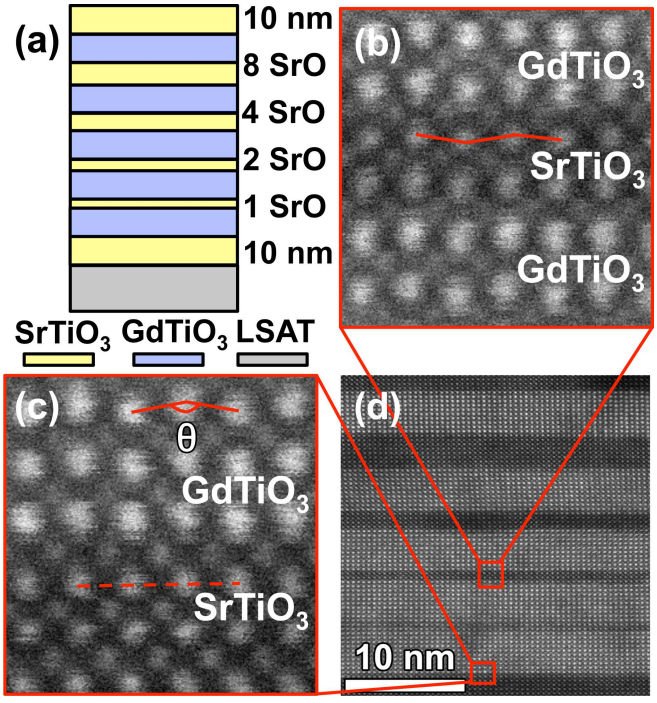

Figure 1 LD14165 17MAY2013

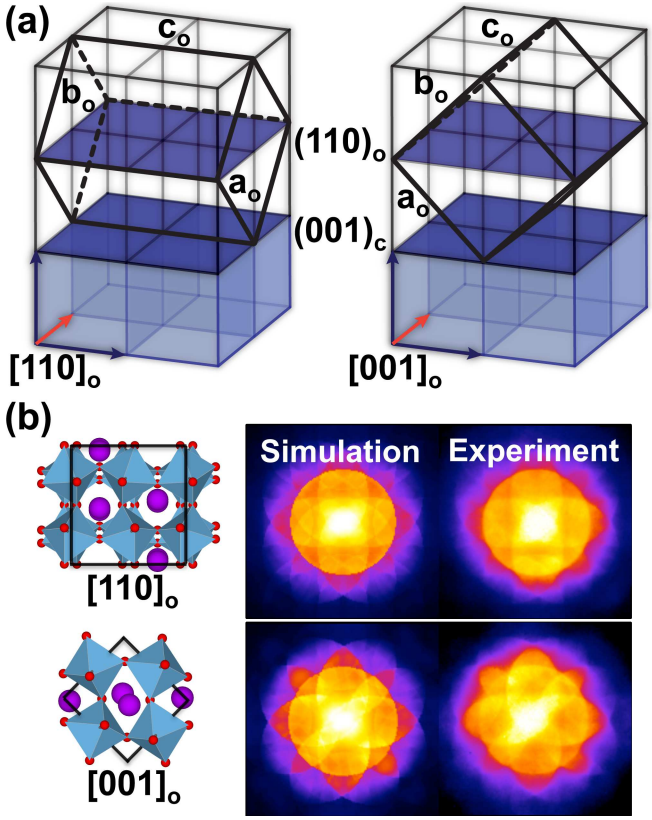

Figure 2 LD14165 17MAY2013

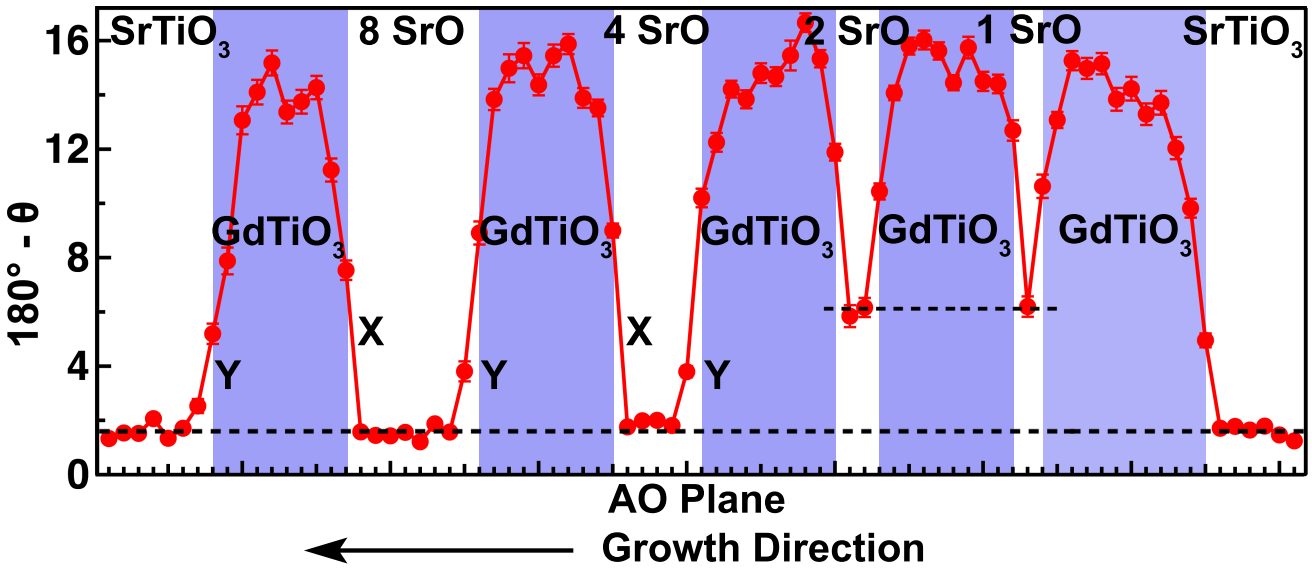

Figure 3 LD14165 17MAY2013

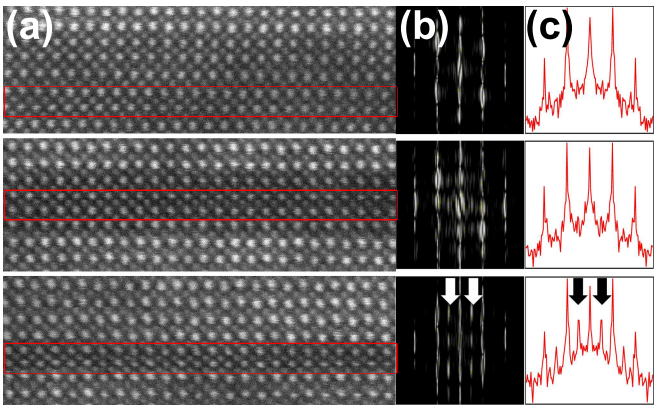

Figure 4 LD14165 17MAY2013